Received: 24 August 2022 | Revised: 6 February 2023 | Accepted: 7 February 2023

DOI: 10.1111/acel.13802

Aging Cell WILEY

RESEARCH ARTICLE

Intestinal stem cell aging at single-cell resolution: Transcriptional perturbations alter cell developmental trajectory reversed by gerotherapeutics

Jiahn Choi[1] | Michele Houston[1] | Ruixuan Wang[2] | Kenny Ye[3] | Wenge Li[1] | Xusheng Zhang[4] | Derek M. Huffman[2,5] | Leonard H. Augenlicht[1,5]

[1]Department of Cell Biology, Albert Einstein College of Medicine, Bronx, New York, USA

[2]Department of Molecular Pharmacology, Albert Einstein College of Medicine, Bronx, New York, USA

[3]Department of Epidemiology and Population Health, Albert Einstein College of Medicine, Bronx, New York, USA

[4]Department of Genetics, Albert Einstein College of Medicine, Bronx, New York, USA

[5]Department of Medicine, Albert Einstein College of Medicine, Bronx, New York, USA

Correspondence
Jiahn Choi, Department of Cell Biology, Albert Einstein College of Medicine, Ullmann 911C, 1300 Morris Park Ave, Bronx, New York 10461, USA.
Email: jiahn.choi@einsteinmed.edu

Funding information
National Cancer Institute, Grant/Award Number: P30-013330, R01CA214625, R01CA222358 and R01CA229216; National Institute on Aging, Grant/Award Number: 5T32AG023475-20 and P30 AG038072

Abstract

The intestinal epithelium consists of cells derived from continuously cycling Lgr5^{hi} intestinal stem cells (Lgr5^{hi} ISCs) that mature developmentally in an ordered fashion as the cells progress along the crypt-luminal axis. Perturbed function of Lgr5^{hi} ISCs with aging is documented, but the consequent impact on overall mucosal homeostasis has not been defined. Using single-cell RNA sequencing, the progressive maturation of progeny was dissected in the mouse intestine, which revealed that transcriptional reprogramming with aging in Lgr5^{hi} ISCs retarded the maturation of cells in their progression along the crypt-luminal axis. Importantly, treatment with metformin or rapamycin at a late stage of mouse lifespan reversed the effects of aging on the function of Lgr5^{hi} ISCs and subsequent maturation of progenitors. The effects of metformin and rapamycin overlapped in reversing changes of transcriptional profiles but were also complementary, with metformin more efficient than rapamycin in correcting the developmental trajectory. Therefore, our data identify novel effects of aging on stem cells and the maturation of their daughter cells contributing to the decline of epithelial regeneration and the correction by geroprotectors.

KEYWORDS
gerotherapeutics, intestinal stem cell aging, intestinal stem cells, metformin, rapamycin, single-cell RNA sequencing

1 | INTRODUCTION

The intestinal mucosa is a prime example of the decline in regenerative capacity, increase in cellular damage and metabolic dysregulation that characterizes aging (Di Giosia et al., 2022). These changes are linked to age-associated intestinal disorders, with aging also a major risk factor for colorectal cancer (CRC) (Nalapareddy et al., 2022). The potential role of perturbations in Lgr5^{hi} intestinal stem cells (Lgr5^{hi} ISCs) is of particular interest in understanding aging since these cells renew and maintain the mucosa through their continuous division at the crypt base (Barker et al., 2007). Reduction in Wnt signaling has been reported as a key that represses stem cell functions of Lgr5^{hi} cells with aging (Nalapareddy et al., 2017; Pentinmikko et al., 2019), but how it links to the developmental progression of progenitor compartments has not been addressed.

Several pharmacologic approaches have been reported to delay age-related manifestations including reversal of stem cell dysfunction and extension of lifespan (Moskalev, 2020; Partridge

et al., 2020). Although none are yet approved for ameliorating the effects of aging in humans, metformin and rapamycin have been studied as regulators of cellular metabolic activities that are linked to aging phenotypes (An et al., 2020; Blagosklonny, 2019; Moskalev et al., 2022; Novelle et al., 2016). However, given their pleiotropic impact on metabolism and linked pathways, understanding the complexity of their effects requires more detailed investigation.

Therefore, we interrogated the complexity of aging effects on the intestinal mucosa and how potent geroprotectors intervene in the effects of aging using single-cell RNA sequencing (scRNAseq) of the intestinal epithelium. Novel cellular and bioinformatic analyses revealed that aging significantly reprogrammed transcriptional profiles of canonical Lgr5^{hi} ISCs and delayed the progression of the developmental trajectory of the cells that produced the progenitor cell compartments. Further, the heterogeneity of cellular response was identified that determines the efficiency of the potential reversal of effects by the geroprotectors, metformin, and rapamycin. The data are incisive in defining how intestinal stem cells and the developmental programs of their progeny are altered with biological aging, identifying key imbalances among the pathways of Wnt signaling, cell cycling, and metabolism as cells undergo stage-specific developmental maturation, and the overlapping but also distinct effects of metformin and rapamycin in correcting these defects in aged mice.

2 | RESULTS

2.1 | Aging reprograms transcriptional profiles that determine the function of canonical Lgr5^{hi} ISCs

Cell programming and function across all cell types and lineages of the intestinal mucosa were dissected in four groups of CB6F1 hybrid male mice, 3 independent mice in each group (Figure 1a): 5-month-old young mice (Y), 24-month-old aged mice (O) fed a purified diet for 3 months beginning at 2 or 21 months of age, respectively, with two additional groups of aged mice also receiving the diet supplemented with either 0.1% metformin (O-met) or rapamycin (O-rap) at 42 ppm for the 3-month period. FACS-isolated intestinal epithelial cells (Epcam+, Cd45neg) were analyzed by scRNAseq (Figure S1a). Known markers aligned 21 cell clusters with cell types and lineages of the small intestine from stem through progenitor cell compartments and then less mature and eventually fully differentiated absorptive and secretory cells (Figures 1b and S1b). The proportion of cells in each cluster/cell type was similar across the different age and treatment groups, suggesting that the overall cellular composition of the intestinal epithelium was maintained for >2 years of age in the mouse (Figure S1c). However, analysis of gene expression demonstrated a wide range of genes altered in expression with age across clusters and lineages (≥1.5-fold change, coupled with P_{adj} <0.01, Figure 1c), suggesting that transcriptomic profiles in the ostensibly same cell types are reprogrammed with age. For most clusters, treatment of the aged mice with metformin or rapamycin reversed altered expression profiles in cells. Restoration of expression profile was most effective in EC8 cells, identified as mature enterocytes, for both drugs, where it had been altered to the greatest extent in the aged mice (Figure 1c; Table S1).

The Lgr5 gene, encoding the receptor for the key stem cell growth factor R-spondin, is regulated by Wnt signaling, and in the intestine, is most highly expressed in cells at the crypt base (Barker et al., 2007). These Lgr5^{hi} cells are considered the major canonical stem cells maintaining the structure and function of the intestinal epithelium (Barker et al., 2007). The mean expression of Lgr5 mRNA in the stem cluster from old mice significantly decreased by 33% compared to that in young mice and was restored back to 87% of young mice by metformin and 83% by rapamycin (Figure 2a). We next focused on Lgr5^{hi} cell signature genes, defined as those genes altered in expression in the immediate Lgr5^{lower} progeny of Lgr5^{hi} cells that have left the stem cell niche and no longer function as stem cells (Muñoz et al., 2012). Of the 467 transcripts in this stem cell signature gene set expressed in Lgr5^{hi} cells from young mice, 71% were expressed at a lower level in older mice (Figure 2b).

The distributions of expression levels in young vs old mice, and in young vs old mice treated with either rapamycin or metformin, are shown in Figure 2c, with the percentage of genes at different levels of expression relative to young mice in Table 1. Compartments 1 and 2 are those Lgr5^{hi} stem cell signature genes repressed by >50% (compartment 1) or 20%–50% (compartment 2, Figure 2c). However, for older mice treated with rapamycin or metformin, this pattern was shifted (Figure 2c; Table 1). Specifically, as shown in Figure 2c with quantification in Table 1, in old mice, 12% of the signature genes were expressed at or less than 50% of their level in young mice (compartment 1), but this decreased to 5% and 4% for the old mice treated with metformin and rapamycin, respectively. Similarly, expression levels for 38% of the signature genes were 20% to 50% lower in old mice (compartment 2), but the percent of signature genes at these lower levels decreased to 30% and 33% for the old rapamycin and metformin-treated mice, respectively. Reflecting this, the number of genes in compartments 3 and 4, in which expression level changes were within 20% of young mice, increased in the old mice treated with rapamycin or metformin (Figure 2c; Table 1). These shifts in the cumulative distribution of gene expression ratio were analyzed statistically using the Kolmogorov–Smirnov test (Massey Jr., 1951). Comparison between Old/Young vs Old-treatment/Young for each drug significantly shifted the distribution closer to 1 (p <0.001 for each drug). However, the comparison between rapamycin and metformin was not significantly different (Figure 2d). Thus, the repressed expression of stem cell signature genes in aged Lgr5^{hi} cells was significantly rescued by treatment with rapamycin or metformin.

Gene set enrichment analysis (GSEA) identified significantly altered pathways in the stem cell cluster (Figure 2e). Oxidative phosphorylation (OXPHOS), a key metabolic pathway in regulating stem cell function (Rodríguez-Colman et al., 2017; Zhang et al., 2022) was upregulated in the stem cell cluster of older mice, and this was reversed by either metformin or rapamycin. Moreover, the linked metabolic pathways of fatty acid metabolism and glycolysis were

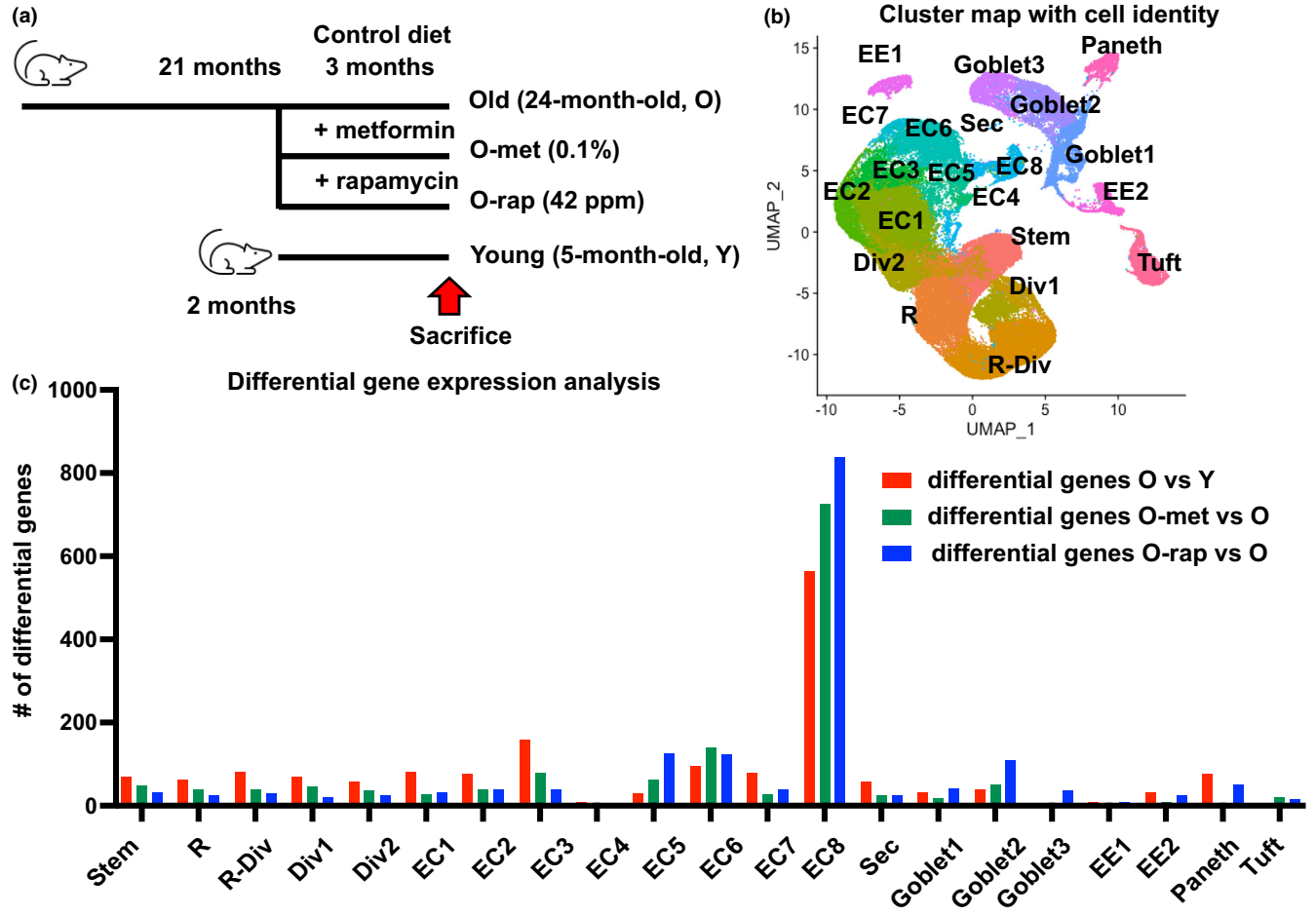

FIGURE 1 scRNAseq analysis of small intestinal epithelial cells: (a) Schematic representation of experimental designs; drug treatment was started at age of 21-month-old for 3 months. 3 replicates were used in each group. (b) Cluster map and cell lineages from 12 combined scRNAseq libraries. Abbreviates; R—replicating; R-Div—replicating to dividing; Div—dividing; EC—enterocytes; Sec—secretory progenitor cells; EE—enteroendocrine cells; (c) number of differentially expressed genes (fold change >1.5 & P_{adj} <0.01) in each cluster from the comparison between old vs young (red bar), metformin-treated vs old (green bar), and rapamycin-treated vs old (blue bar)

also upregulated in the stem cluster of old mice but reversed only by metformin treatment. By contrast, Wnt and cell cycle pathways, which are fundamental for stem cell self-renewal and generation of progeny that undergo differentiation, were suppressed in the stem cluster of old mice, while the ribosome pathway, also important for supporting stem cell function, and downregulated as cells mature during their migration along the crypt-villus axis (Mariadason et al., 2005) was upregulated in the stem cells. Thus, although it is established that OXPHOS is necessary for ISC functions (Rodríguez-Colman et al., 2017), the elevation of this and related fatty acid metabolism in older mice may also perturb stem cell functions, emphasizing the importance of maintaining these pathways within a homeostatic range for normal stem cell functions. This was confirmed by investigating the self-renewal capability of stem cells by analysis of BrdU incorporation prior to sacrifice (Figure S2a). Quantification of BrdU+ nuclei in crypts confirmed that proliferating cells were reduced in old mice by 28% (p <0.0001; Figure S2b). Metformin or rapamycin treatment increased proliferating cells back to youthful levels, both highly statistically significant (Figure S2b), confirming that the proliferation of ISCs was suppressed both transcriptionally and functionally, which were rescued by drug treatments.

Single-cell analysis enables investigating the link between the essential and altered pathways in individual cells. This was investigated using the AddModuleScore function, which calculates the activity score for a pathway in individual cells by accessing gene expression level compared to random control genes (Tirosh et al., 2016). Figure S2c illustrates the correlated distribution of Wnt and cell cycle pathways in individual ISCs (left) and Lgr5^{hi} ISCs (right) for each condition, the elliptical areas delineating points within 95% of the Gaussian distribution. This shifted towards the lower left with aging but was partially reversed by rapamycin and metformin back towards the informatic space occupied by younger mice. By contrast, coordinate regulation of the ribosome (protein synthesis) and cell cycle pathways showed that the module score was higher for ribosome activity with lower cell cycle activity in aged mice, but the effect of either rapamycin or metformin treatment to shift these back towards the pattern of young mice were less clear (Figure S2d). Bivariate analysis using MANOVA for two variables based on mean module

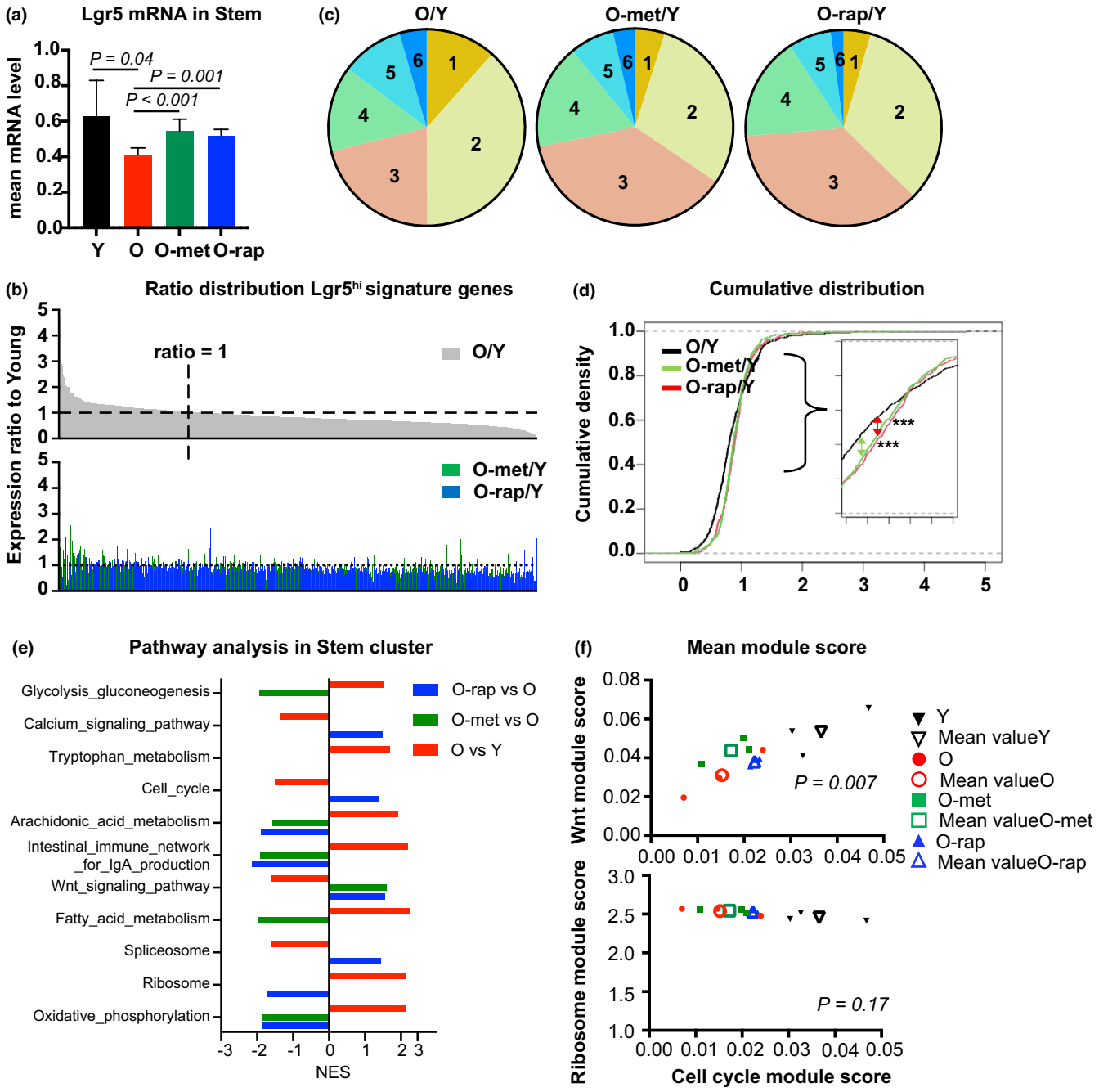

FIGURE 2 Impact of aging on function of intestinal stem cells: (a) average mRNA expression of the *Lgr5* genes in the Stem cluster. (b) Expression ratio of old vs young of 467 genes of an Lgr5^{hi} ISC signature (Muñoz et al., 2012), and corresponding ratio of old-met vs young or old-rap vs young (lower panel). (c) Distribution of genes as a function of the ratio of expression; corresponding ratios in Table 1. (d) Cumulative density graph of ratio distribution. Statistical analysis was performed using the Kolmogorov–Smirnov test between two groups (***: $p < 0.001$). (e) Differentially-regulated pathways ($P_{adj} < 0.05$) in the stem cluster using GSEA KEGG pathways; NES—normalized enrichment score. (f) Scatter plot for two variables with mean module score. Mean module scores from each mouse (filled) or each condition (empty, average value) were plotted for Wnt and cell cycle pathways (top) or ribosome and cell cycle pathways (bottom). *p* value was calculated using MANOVA, assuming each mouse as independent.

score showed that the Wnt and cell cycle pathways were positively correlated and significantly different among all experimental groups, demonstrating that Wnt and cell cycle pathways are coordinated in individual cells and average activities in the stem cluster shifted significantly among groups (Figure 2f; $p = 0.007$). However, ribosome and cell cycle pathways were not clearly coordinated among all groups (Figure 2f). Thus, for cells in the ISC compartment overall, and specifically for the Lgr5^{hi} ISCs, the Wnt and cell cycle pathways are both regulated coordinately and significantly suppressed by aging but enhanced ribosomal activity in aged mice is discordant with the repressed cell cycle pathway, suggesting a perturbed balance between protein synthesis and cell cycle in aged ISCs.

TABLE 1 % Lgr5 signature genes in range

	Expression ratio	O/Y	O-met/Y	O-rap/Y
1	0–0.5	12%	5%	4%
2	0.5–0.8	38%	30%	33%
3	0.8–1	21%	37%	36%
4	1–1.2	14%	17%	17%
5	1.2–1.5	10%	7%	7%
6	>1.5	4%	4%	2%

2.2 | Altered metabolism of ISCs influences their essential functions

With the fact that aging perturbs the self-renewal capability of Lgr5^{hi} cells, and metabolic changes of ISCs influence how their progeny mature and undergo lineage differentiation (Alonso & Yilmaz, 2018; Beumer & Clevers, 2020; Chandel et al., 2016), we extended analyses to how these cells mature as they progress through progenitor and lineage-specific compartments. Pathway analysis using fold change of differentially expressed genes in old vs young mice showed that at least 79% of the significantly altered pathways in ISCs of old mice continue to be altered in the progenitor cell types sequentially emerging from the stem cell compartment (Figure S3a). This included the compartments identified as Replicating (R), Replicating-Dividing (R-Div), and Dividing 1 and 2 (Div1, Div2). Therefore, we hypothesized that changes in stem cell expression profile can continue to influence the progressive maturation of cells as they progress through these cell compartments. This was analyzed using Monocle, which predicts the trajectory of cell maturation based on gene expression profiles in individual cells (Trapnell et al., 2014). Assuming cells derived from the Stem cluster (yellow arrow, Figure S3b), monocle established a trajectory from Stem through intermediate cell types towards enterocytes for the young mice (Figure S3b). Spatial markers that have been shown to identify cell position along the crypt-villus axis (Moor et al., 2018) confirmed that the predicted trajectory was well aligned with the physical positioning of lineage development along the crypt-villus axis (Figure S3c), including the Monocle prediction of EC8 cluster that exclusively expressing villus tip markers at the end of the trajectory. Similar trajectories were predicted for both young and old mice, irrespective of drug treatment. This is consistent with the data that cell-type representation was well conserved among all the groups (Figure S1c). To follow cell progression, cells were selected along the trajectory from the stem cell origin (yellow arrow) to the point at which the daughter cells have traversed the progenitor cell compartments to give rise to enterocytes (green arrow, Figure S3b, individual cells color-coded either green or pink in Figure 3a). Along this portion of the trajectory, there was a main developmental route and branches coming off along the route. To interrogate how cellular characteristics differed depending on their position along the trajectory, cells were dichotomized into the mainstream (main, green color) and side branch cells (side, pink color) (Figure 3a). Module scores for the pathways identified in Figure 2e were calculated as previously described to compare the main and side branch cells of each mouse group (Figure 3b–i). Strikingly, violin plots of module scores clearly showed that the alterations induced by aging were principally derived from mainstream cells along the path of developmental cell maturation. For instance, distribution and average module scores for four pathways (Wnt, cell cycle, ribosome, and OXPHOS) for main cells were significantly different among all groups (ANOVA, Figure 3b–e), but module scores of the same pathways for the side cells differed for cell cycle and OXPHOS but not for Wnt or ribosome pathways among groups (Figure 3f–i). Further analysis by the Tukey's multiple comparison test (Table S2) interrogated the individual group comparisons for each pathway independently for both main and side stem cells. Based on the adjusted p value (Table S2), the impact of aging for three pathways related to stem cell functions was significantly different for the main trajectory cells, not for the side cells. Interestingly, dichotomized analysis of metformin-treated mice demonstrated elevation of cell cycle activities in these main stem cells, which was not significantly different when analyzed for total stem cell population, suggesting a heterogeneous response to the drug within the same cluster. Rapamycin also elevated these pathways in the main stem cells of old mice but only the cell cycle pathway was significantly reversed (Figure 3b–d; Table S2). This analysis also revealed that OXPHOS activity differed based on cell position on the trajectory. In the main stem cells, there was a steep difference in mean module score between young and old mice, but the difference did not exist in the side stem cells, implying that aging impaired the balance of metabolic activity determining the function of ISCs (Figure 3e,i). Elevation of OXPHOS in main stem cells from old mice was reversed towards that of young mice with metformin, but rapamycin was not effective for main stem cells, rather affecting side stem cells, reflecting the overall lower efficacy of rapamycin and the distinct mechanisms of action of the two drugs (Figure 3e,i, Table S2). Thus, this rigorous bioinformatic-statistical analysis shows that activities of key cellular functions and metabolic pathways are distinct in relation to position along the intestinal cell developmental trajectory in young mice, compared to old mice. Metformin and rapamycin treatment both augmented key pathway activities. However, metformin showed a greater effect on adjusting key pathways in main cells, while the rapamycin effect was less dependent on the cellular position along the trajectory.

2.3 | Alteration in stem cells delays proper maturation of cells

Analysis of disease pathways for the mainstream cells along the trajectory using Ingenuity Pathway Analysis (IPA) revealed that the stem and progenitor clusters along the trajectory in old mice showed activation of the predefined pathways of organismal death, growth failure, and apoptosis, and complementary inhibition of cell survival pathways, consistent with the potential deteriorating function of the tissue with age (Figure 4a–d). These pathogenic pathways reversed

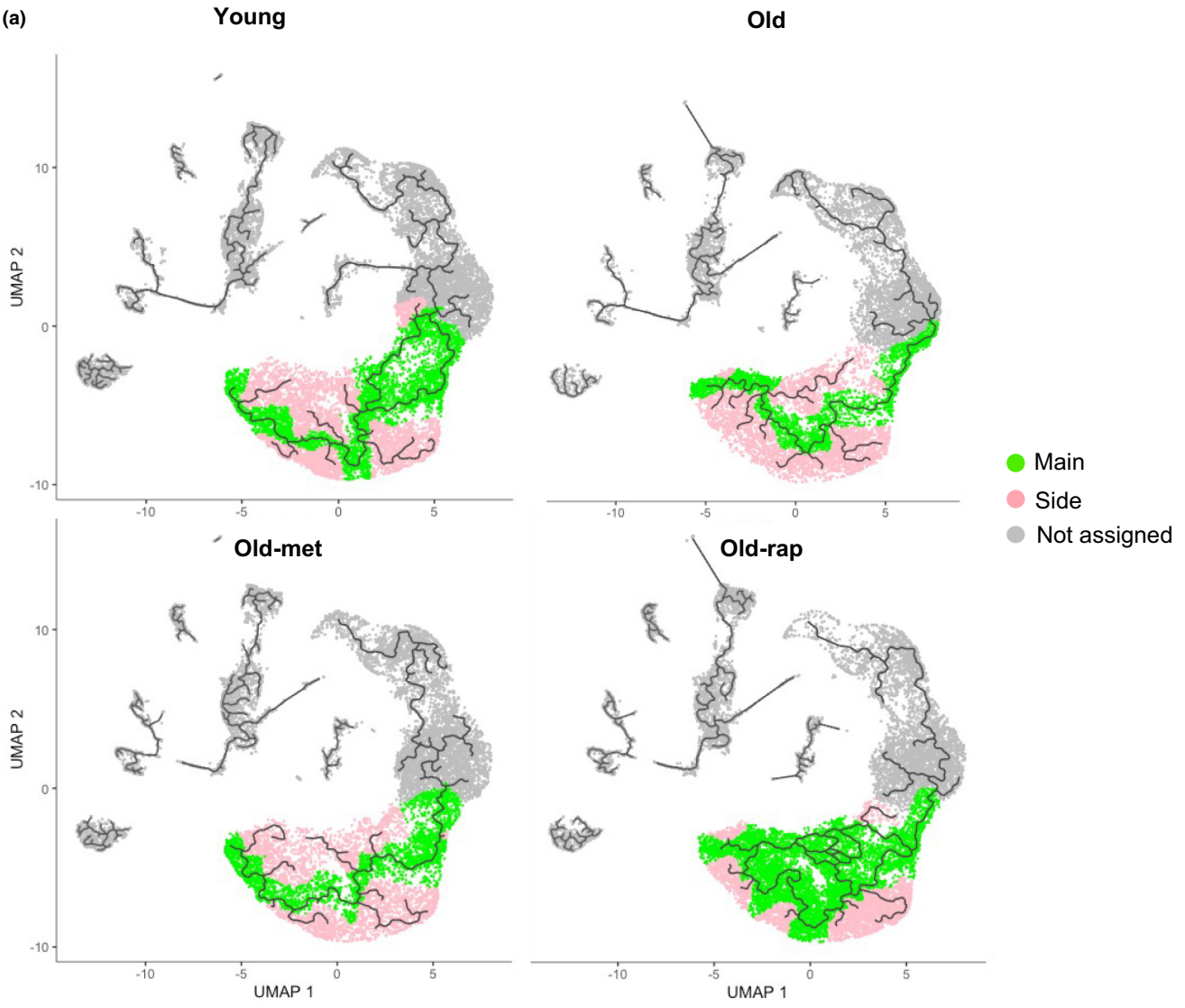
(a)
Young
Old
Old-met
Old-rap
UMAP 2
UMAP 1
Main
Side
Not assigned

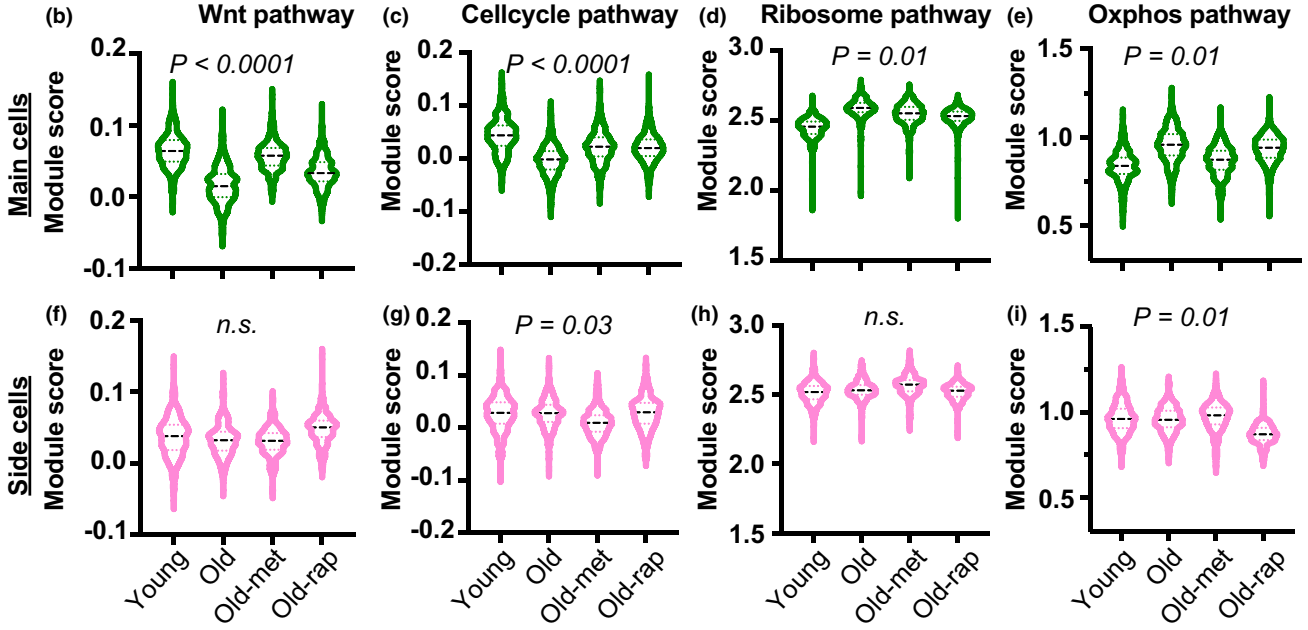
(b) Wnt pathway
(c) Cellcycle pathway
(d) Ribosome pathway
(e) Oxphos pathway
(f)
(g)
(h)
(i)
Main cells
Side cells
Module score
P < 0.0001
P < 0.0001
P = 0.01
P = 0.01
n.s.
P = 0.03
n.s.
P = 0.01
Young
Old
Old-met
Old-rap

FIGURE 3 Impact of aging on stem cells differs depending on the position along the trajectory: (a) trajectory graph for each condition. Based on the position of each cell along the trajectory, cells on main track color-coded green, and cells on side branches color-coded pink. Cells not included in the analysis are color-coded gray. (b–i) Module scores of four different pathways plotted separately by position (main: b–e, side: f–i) on the track and condition. Statistical significance was determined by the ANOVA test and applied for each position separately.

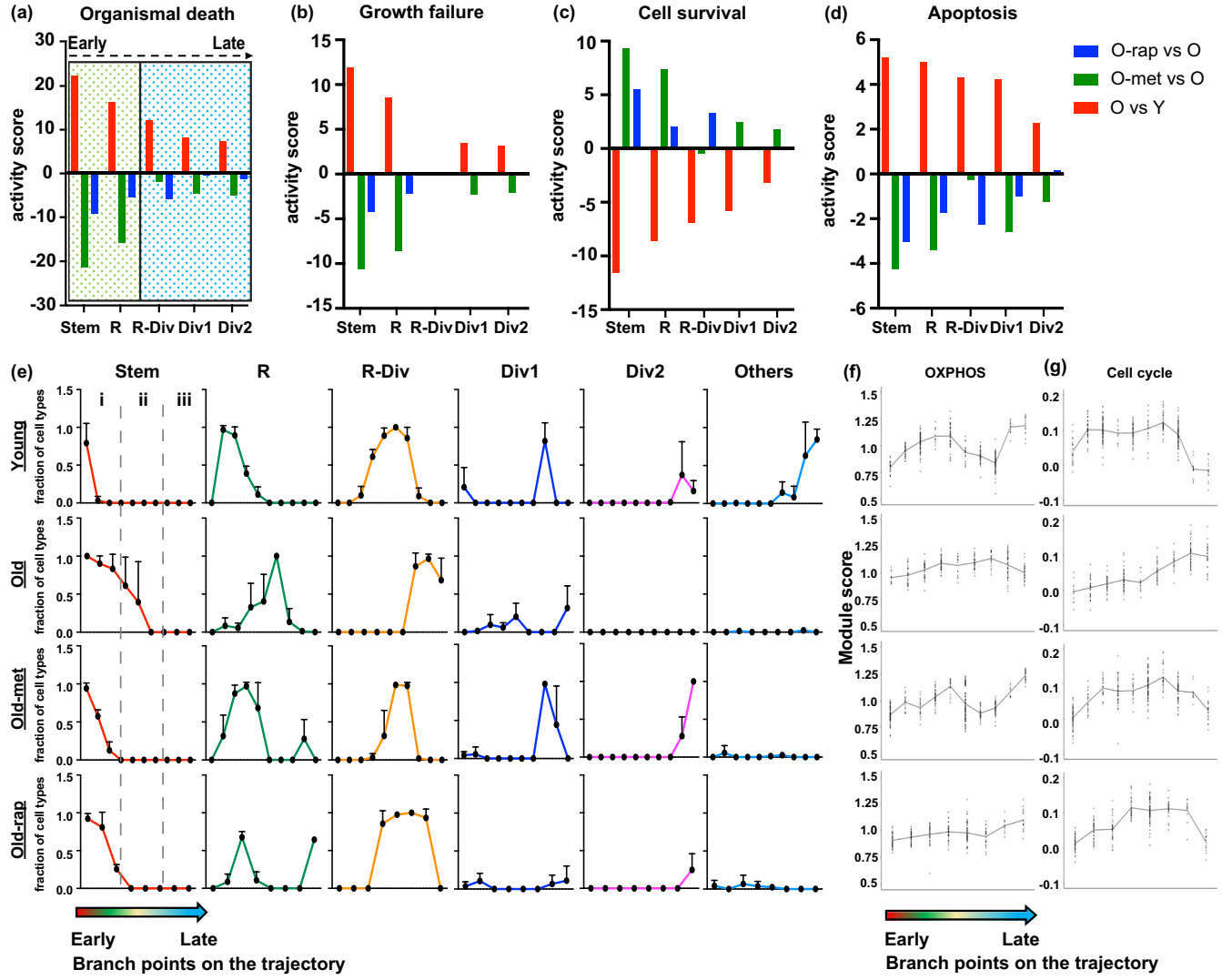

FIGURE 4 Aging delays proper cell maturation along the developmental trajectory: (a–d) assignment of disease pathway based on differentially expressed genes (P_{adj} <0.05) in main cells of Stem and subsequent progeny clusters were analyzed using QIAGEN IPA (QIAGEN Inc., https://digitalinsights.qiagen.com/IPA). Dotted green box indicates cell types assigned to clusters early in the trajectory (Stem and R); dotted blue box indicates cell types later in the trajectory (R-Div, Div1, and Div2). (e) Cell-type transition along the branch points of the trajectory plot. Dashed line indicates compartments that divide the trajectory into three segments (early(i), mid(ii), and late(iii)). This compartmentalization was utilized for statistical analysis of the alteration of cell identity along the developmental trajectory under the different conditions using the Pearson's chi-squared test. The analysis confirmed that cell-type distribution in each compartment is significantly different (compartment i: $p = 0.001$; compartment ii: $p = 0.04$; compartment iii: $p = 0.015$). (f) Module score of OXPHOS pathway at each branch point analyzed for cell-type transition in e. (g) Module score of cell cycle pathway at each branch point analyzed for cell-type transition in e

in the stem and R clusters (early cell type along the developmental trajectory) of old mice by treatment with either metformin or rapamycin (Figure 4a–d). However, further downstream in the developmental trajectory (R-Div, Div1, Div2) and the efficacy of the two drugs diverged, with metformin significantly more effective in reversing the pathway changes with age (Figure 4a–d). Therefore, we extended the informatic analysis to how cell maturation was altered by aging and drug treatment throughout the developmental trajectory of the cells by interrogating cells on the branching points between sequential compartments in the trajectory. This

was done for cells informatically identified as Stem, R, R-Div, Div1, Div2, and Others, the latter encompassing later differentiated cells (Figure 4e). Each of these cell types emerged sequentially in Young mice along the trajectory (Row 1, Figure 4e). However, in Old mice (Row 2), there was a clear delay in the position along the trajectory at which the development of each cell type was detected. Strikingly, metformin treatment (Row 3) restored the appearance of cell type to a more youthful position all along the trajectory. Rapamycin was similarly effective, with the exception of Div1 cells, which did not differ from Old mice (Row 4) in line with its lower efficiency on later cell types rescuing pathogenic pathways in Figure 4a-d. To perform statistical analysis, we divided branch points into 3 compartments (Figure 4e, i–iii). Cell-type distribution in each compartment was compared across the conditions using Pearson's Chi-squared test with simulated p value. Individual comparison of each compartment confirmed cell-type distribution is significantly different, including when each was considered independently (compartment i: $p = 0.001$; compartment ii: $p = 0.04$; compartment iii: $p = 0.015$). When all compartments were considered together, the p value was <0.0001, supporting our hypothesis that cell-type transition along the branch points significantly changed with aging.

The relationship between the OXPHOS and cell cycle pathways was investigated along this trajectory using a module score for each pathway as in the earlier analyses. In young mice, the mean module score for OXPHOS between branch points (Figure 4f) gradually increased and then decreased along with the cell-type transition of the developmental trajectory, and showed a sharper rise at the last 2 stages of the trajectory where mature cells initially appear. However, this pattern was greatly attenuated in Old mice. Metformin restored the pattern towards that of young mice, but rapamycin did not. Similarly, for the cell cycle pathway (Figure 4g), the mean module score increased as the cells emerged from the stem cell compartment, in parallel to known elevated proliferation in subsequent compartments, collectively termed the transit amplifying cells, and then fell sharply at the end of the trajectory in accordance with the appearance of mature enterocytes. By contrast, there was a progressive increase in the cell cycle module score along the trajectory in Old mice, but the sharp decrease at the end of the trajectory seen for Young mice did not occur, suggesting an incomplete process of maturation until the last branch point on the trajectory. However, both metformin and rapamycin restored this overall pattern in old mice to more closely resemble the temporal pattern at these stages in young mice. In summary, our data show a tight linkage between predicted cell identity and metabolic pathways in cell maturation along the developmental trajectory of intestinal epithelial cells, and that aging perturbs the coordination of how these cells are reprogrammed, which leads to this impaired developmental progression of cells. We further investigated the increased OXPHOS pathway using IHC for Ndufb8 of complex I and Cox5b of complex IV of the mitochondrial electron transport chain. Quantitative analysis showed that both Ndufb8 and Cox5b were significantly elevated in the crypts of old mice compared to young mice, consistent with scRNAseq analysis (Figure S4a–d). Interestingly, neither metformin nor rapamycin reversed these changes at the protein level. The discrepancy in the effect of the drugs between the level of RNA expression of nuclear genes encoding these mitochondrial proteins and its protein level may be due to the fact that mitochondria are long-lived, and that 3 months of treatment with the drugs is not sufficient to alter their structure, whereas in the old mice, substantial remodeling of mitochondria is accumulated with age.

Analysis of the single-cell data had shown a clear delay of cell maturation along the developmental trajectory with aging and its reversal by geroprotectors. This was followed up by an investigation of two specific genes using immunofluorescence. *Uhrf1* and *Ccnb1* were assayed since their expression level was tightly associated with cell identity: *Uhrf1* is highly expressed in early progenitor cells, but *Ccnb1* is highly expressed in later progenitors. In addition, there was a clear delay along the trajectory for expression of each of these genes in old mice compared to young mice, while either metformin or rapamycin treatment restored the pattern similar to in young mice (Figure 5a). Therefore, we hypothesized that cells co-expressing both genes are intermediate cells that undergo differentiation from early to later progenitor cell types. Staining for the proteins encoded by each gene showed enriched expression in the crypt that confirmed their expression in progenitor cells (Figure 5b). Cells positively stained for each protein were then analyzed to calculate the percentage of cells co-stained for both proteins (Figure 5c). One-way ANOVA followed by Tukey's multiple comparison confirmed that there are significantly more cells co-stained for both proteins in old mice than in young mice, supporting the conclusion that cell maturation along the crypt-villus axis is retarded by aging. Consistent with trajectory analysis, metformin treatment showed a significant decrease in the number of co-stained cells, but this decrease was marginal for rapamycin in keeping with its less pronounced effects (Figure 4e). Thus, these data independently confirm the more extensive bioinformatic analyses.

3 | DISCUSSION

Transcriptomics at single-cell resolution establish that aging suppressed expression of the Lgr5 gene in the intestinal stem cluster by >30% and repressed expression of >70% of the genes reported as the transcriptional signature defining Lgr5^{hi} stem cells (Muñoz et al., 2012). Lgr5 is a Wnt target gene and a receptor for R-spondin, a functional driver of cycling ISCs, and we documented downregulation of Lgr5 expression in line with the repression of Wnt signaling pathways in stem cells of the aged mice. Therefore, aging may compromise sustained self-renewal and the ability of these canonical stem cells to produce progeny and maintain mucosal function. This extensive downregulation of the stem cell signature genes in Lgr5^{hi} cells begins as early as middle age (12-month-old mouse) in comparison to young adults (3-month-old, data not shown). Thus, these data support reports that aging impairs the primary stem cells in the small intestine both functionally and transcriptionally (Cui et al., 2019; Nalapareddy et al., 2017).

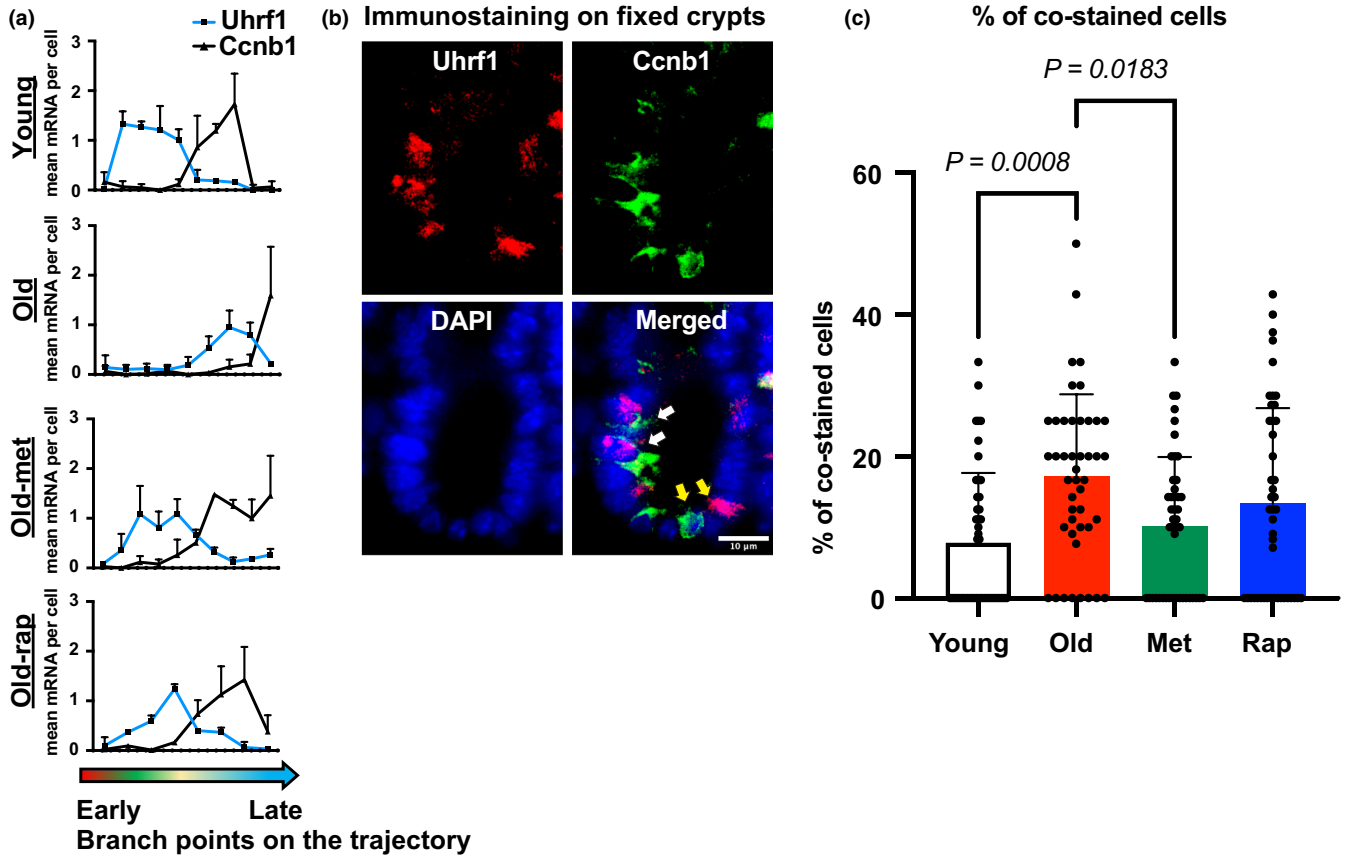

FIGURE 5 Retardation of developmental trajectory is reflected in cell maturation process: (a) mean mRNA expression of Uhrf1 and Ccnb1, which expression level changes along with developmental trajectory. (b) Representative images of IF for proteins encoded by Uhrf1 or Ccnb1 in FFPE tissues. Images show cells stained with either protein alone (yellow arrows) or cells co-stained for both proteins (white arrows). Scale bar: 10 μm. (c) Quantitation of co-stained cells in each condition. 15 crypts were analyzed from 3 mice of each condition. Statistical analysis was performed using one-way ANOVA followed by Tukey's multiple comparison.

Metabolic pathways are critical for sustaining continuous cell cycling of Lgr5^{hi} ISCs to maintain the mucosa, and metabolic status is also a key in determining whether stem cells retain self-renewal capacity or differentiate following their replication (Mihaylova et al., 2018; Rodríguez-Colman et al., 2017; Wang et al., 2021). Our data show that aged mice exhibited significant alterations in key metabolic pathways such as OXPHOS, glycolysis, and fatty acid metabolism. Therefore, the programming of metabolic pathways is reconfigured in aging with important consequences for stem and progenitor cell functions and mucosal remodeling. Dichotomized analysis clearly showed that there was heterogeneity even among cells within the same cluster as regards to metabolic pathway profile. In young mice, stem cells exhibited lower expression of the OXPHOS machinery consistent with elevated cell cycle and Wnt pathway activities, while in old mice, OXPHOS was elevated in stem cells, in conjunction with suppression of Wnt and cell cycle pathways. Importantly, the unique architecture of the mucosa permits linking these alterations to the developmental progression of the stem cell progeny. In this regard, the distinct metabolic activities linked to cell position along the crypt-luminal axis emphasizes that coordination between metabolism and stem cell functions is fundamental for normal stem cell functions, and that the disruption in aged mice alters the acquisition of cell identity during the progression of cells along the mainstream of their developmental maturation. We have previously suggested this fundamental link is through altered mitochondrial function (Augenlicht & Heerdt, 2001), and more recently have shown this is a key to nutritional remodeling of ISCs and mucosal homeostasis that establishes elevated probability for development of sporadic tumors (Choi et al., 2022).

Metformin and rapamycin are gerotherapeutics under intense investigation for their potential to delay many facets of aging to ameliorate physiological deterioration and potentially increase the quality and length of life (Harrison et al., 2009; Martin-Montalvo et al., 2013; Novelle et al., 2016). Both pharmacological agents reversed multiple aspects of the aging transcriptomic phenotype in the intestinal mucosa. At doses shown to extend mouse lifespan, each drug suppressed OXPHOS and augmented Wnt signaling (Figure 2e). Importantly, there were distinct differences in their impact on cell programming, with metformin more effective in adjusting metabolic pathway expression signatures by reducing the aging-associated effect on fatty acid oxidation and glycolysis while rapamycin more directly enhanced proliferation (Figure 2e). Further dissection of their distinct effects using dichotomized analysis revealed that the effect of metformin was concentrated on the main cells that drive

developmental progression, while the effect of rapamycin was less tightly linked to their position on the trajectory. Therefore, tracing cellular maturation using trajectory analysis showed that metformin-treated mice restored the profile of developmental progression that characterizes the mucosa of young mice, while the effect of rapamycin was more limited. Trajectory analysis is a novel approach to understand the more subtle effects on cell developmental maturation in aging, and similar trajectory analyses based on transcriptional profiles have also recently been used to show altered cell differentiation along the crypt-luminal axis in human ulcerative colitis (Smillie et al., 2019), in ISCs in which mitochondrial composition has been altered (Ludikhuize et al., 2020), and in mice fed a diet that increases the probability for tumor development (Choi et al., 2022).

Aging is a major underlying risk factor for CRC (Nalapareddy et al., 2022), with clear effects of aging on the intestine reported (Baron & Pisani, 2021; Choi et al., 2018; He et al., 2020), and herein deconvolved by single-cell analyses. Of note, despite a major disruption in stem cell function and development of linages, older wild-type mice do not develop tumors spontaneously when fed control diets. However, when wild-type mice are fed a diet long-term that mimics intake levels of common nutrients linked to those consumed in populations at high risk for colon cancer, they do develop small and large intestinal tumors reflecting the etiology, incidence, frequency, and lag with older age of human sporadic colon cancer (Aslam et al., 2010; Newmark et al., 2001; Newmark et al., 2009; Yang et al., 2008). This emphasizes that long-term dietary patterns and aging are inextricably linked as major risk factors for the development of human CRC. In the dietary model in which sporadic tumors do develop, there is suppressed function of $Lgr5^{hi}$ ISCs with alternate *Bmi1*+, $Ascl2^{hi}$ cells mobilized that remodel the mucosa and establish pro-tumorigenic chronic inflammation (Choi et al., 2022; Li et al., 2019; Newmark et al., 2009). While aging also had a major impact on suppressing $Lgr5^{hi}$ ISCs, there was no evidence that Bmi1+ cells were mobilized or other potential alternative stem cells recruited. This raises the important question of how aging and long-term consumption of a relevant high-risk diet interact in altering mucosal stem cell functions and physiology in establishing the risk of colon cancer, a disease that dramatically rises in older individuals. Moreover, since geroprotectors such as metformin and rapamycin hold promise for mitigating age-related alterations of the intestinal epithelium, the potential interaction of such drugs with dietary interventions need to be explored for efficacy in mitigating aging-related intestinal stem cell programming and lineage differentiation, and in preventing disease that limits the quality of life and lifespan.

4 | METHODS

4.1 | Animals and experimental design

CB6F1 hybrid male mice were obtained at either 2 or 21 months of age from the NIA-aged rodent colony. On arrival, young (Y) mice were immediately switched to a purified control diet and old (O) mice were randomized to either the same control diet or a diet in which either 0.1% metformin (Cayman Chem) or microencapsulated rapamycin (eRapa) at a concentration of 42 ppm (Rapamycinholdings, Inc.) was incorporated into the formulation (TestDiet). Eudragit was also included in the control and metformin diets (429 ppm) in order to match the rapamycin formulation. All mice were group housed and fed these diets for 3 months under a 14 L:10D photoperiod at 22°C, remained on these formulations for 3 months, and were subsequently euthanized, and intestinal tissue was harvested at either 5 or 24 months of age, respectively, for analysis. 3 replicates for each group were used. All experimental methods were approved by the IACUC at the Albert Einstein College of Medicine.

4.2 | Single-cell RNAseq

Mice were sacrificed, excised intestines opened longitudinally, rinsed with cold saline, single-cell suspensions prepared, re-suspended in antibody staining buffer, blocked with FcR Blocking Reagent (Miltenyi Biotec, 130-092-575), washed and pelleted, then incubated for 20 min at 4°C with, EpCAM-APC (Miltenyi Biotec, Cat No. 130-102-234) and CD45-PerCP (Miltenyi Biotec, Cat No. 130-102-469). Cells were sorted by FACs on a MoFlo instrument and Epcam-positive, CD45-negative total epithelial cells collected.

scRNAseq libraries were constructed by the Albert Einstein Genomics Core using the 3′ kit protocols of 10X Genomics (San Francisco, CA) with approximately 10,000 single FACS collected epithelial cells from each mouse processed on a Chromium Chip B microfluidic apparatus (10X Genomics). Library quality was verified by size analysis of transcripts (BioAnalyzer; Agilent) and after passing quality control assays, multiple libraries were multiplexed and sequenced by HiSeq PE150 using pair-end sequencing, with a readout length of 150 bases (Novogene; Sacramento), and the data assigned to individual cells using the sample indexes.

For sequence alignment and subsequent analysis, output Illumina base call files were converted to FASTQ files (bcl2fastq), these from each mouse aligned to the mouse mm10 genome v1.2.0 and converted to count matrices (Cell Ranger software v3.0.2). 5000–8000 individual cells were identified for each sample, and unique molecular identifiers (UMI) were used to remove PCR duplicates. Quality control and downstream analyses were done in R v4.1.2, using Seurat package v4.1.0(Stuart et al., 2019). To discard doublets or dead cells, cells with gene counts <200 or >5000, or a mitochondrial gene ratio > 20%, were filtered out. Cells from different samples were integrated using Seurat FindIntegrationAnchors and IntegrateData functions, and clusters were identified from the integrated data set using the Seurat FindClusters function. This calculates k-nearest neighbors according to principle component analysis, constructs a shared nearest neighbor graph, and then optimizes a modularity function (Louvain algorithm) to determine cell clusters. Cell clusters were identified using established cell-type markers for intestinal epithelial cells

and cluster markers were identified using Seurat FindMarkers function. Differential gene expression compared samples among experimental groups: initial criteria were an expression change of ≥1.5-fold with associated adjusted *p* value of <0.01 in group comparison (Seurat FindMarkers function). Pathway analysis was performed on differentially expressed genes using clusterProfiler R package v4.2.2; gene set enrichment analysis (GSEA) used the fgsea R package (v1.20.0), and the MSigDB (v5.2) KEGG pathway database. Pathways at Adj $p < 0.05$ were considered statistically significant. Trajectory analysis was done using Monocle3 R package v1.2.6 (Trapnell et al., 2014) with cluster information and cell-type identifications migrated from Seurat using an in-house developed code. The integrated data set was divided among different experimental conditions, and trajectories were generated for each condition. Module score to determine the average expression of the gene set for each pathway was calculated with Seurat AddModuleScore function(Tirosh et al., 2016). Same gene list for KEGG pathway analysis was used.

4.3 | Immunohistochemistry

For BrdU staining, immunostaining was performed as previously described. Briefly, antigen retrieval was performed via a citrate buffer (pH = 6) using a pressure cooker for 10 min. After rehydration and blocking endogenous peroxidase by 3.0% H_2O_2 for 5 min, avidin and biotin blocking (Vector Labs SP-2001) was performed each for 15 min with a wash step in between. Next, slides were blocked and stained using a mouse-on-mouse (M.O.M) kit (Vector Labs BMK-2202) with an antibody against BrdU (1:200; cat#5292, Cell Signaling) following the manufacturing protocol. Slides were then incubated with biotinylated secondary antibody for 30 min, followed by a streptavidin-HRP detection system (Vector labs PK-4000) and application of 3, 3′-diaminobenzidine (DAB) for visualization of the antigen–antibody complex (Scytek). For Uhrf1 and Ccnb1 staining, Swiss roll sections were de-waxed, rehydrated, endogenous peroxidases blocked (3% hydrogen peroxide in methanol), and heat-induced epitope retrieval done with 10 mM sodium citrate buffer (pH 6.0) for all antibodies. After blocking for 1 h, tissues were incubated overnight at 4°C with primary Uhrf1 antibody (Thermo Fisher Scientific, 1:500 dilution of Cat #PA5-29884) and primary Ccnb1 antibody (Thermo Fisher Scientific, 1:500 dilution of Cat #MA1-155). Secondary antibody was incubated for 30 mins on the following day (Goat anti-Mouse DyLight™ 488 (Cat #35502) for anti-Ccnb1, Goat anti-Rabbit DyLight™ 594 (Cat #35560) for anti-Uhrf1 from Thermo Fisher Scientific. 1:100 dilution). Prolong gold with DAPI was used to mount the slide. For subunit protein staining of OXPHOS pathway, the same procedure for IHC staining was performed. Primary antibodies were used at 1:200 concentration for overnight at 4 °C (anti-Ndufb8: ab192878; anti-Cox5b: NBP2-92927). Secondary antibody was incubated for 30 mins (goat anti-rabbit, 1:100).

4.4 | Image analysis

All image analyses were done with Fiji software. To quantify BrdU+ nuclei, duodenal epithelium was imaged at 60x magnification. Automatically set threshold was applied to count BrdU+ nuclei. 15 crypts were measured from 3 individual mice in each group. A number of positive nuclei were divided by the total nuclei in the crypt. To quantify co-stained cells for Uhrf1 and Ccnb1, the duodenal epithelium was imaged at 60x magnification. Nuclei that were positive for fluorescent signal (above top 4% of threshold) were counted, and the percentage of co-stained cells was calculated over the sum of the number of cells positive for each staining. 15 crypts were analyzed from 3 individual mice in each group. To quantify OXPHOS subunit proteins, duodenal and jejunal crypts were imaged at 20x magnification. Automatically set threshold was applied to measure positive areas for signal. The area above the threshold was then divided by the total area of crypt. Measurement was conducted up to 60 μm from the bottom of the crypts to minimize size variability. 17 crypts from 3 mice were measured. One-way ANOVA followed by the Tukey's multiple comparisons test was applied to calculate *p* value. Statistical analysis was performed using GraphPad Prism version 0.3.1 for Mac, GraphPad Software, San Diego, California USA, www.graphpad.com.

4.5 | Statistical analysis

Differences in gene expression between groups (Figure 2a) were modeled by a negative binomial mixed effect model with the number of read counts of individual cells as the response, offset by the number of the total counts of the cells, and the individual mice are treated as random effects. The computation is performed by R function glmer.nb. Two-sample Kolmogorov–Smirnov test was used to compare two distributions (in Figure 2d). Multivariate analysis of variance was used to compare mean module scores at two pathways among the four experimental groups (in Figure 2f) using R function MANOVA assuming each mouse was independent.

Figure 3b-i was tested using one-way ANOVA followed by the Tukey's multiple comparison test (Table S2), which was performed using GraphPad Prism version 0.3.1 for Mac, GraphPad Software, San Diego, California USA, www.graphpad.com. Figure 4e was tested using Pearson's Chi-squared test with a simulated *P* value. Individual comparison of each compartment treated each mouse as independent. Figure 5c was tested using one-way ANOVA followed by the Tukey's multiple comparison test.

AUTHOR CONTRIBUTIONS

L.H.A., D.M.H., and J.C. designed the experiments and supervised the work. K.Y performed the statistical analysis. J.C. performed the data analysis, generated the figures, and wrote the manuscript. J.C., R.X., M.H., and W.L. performed the experiments, and X.Z. performed data processing. All authors contributed to edit the manuscript.

ACKNOWLEDGEMENTS

Supported in part by P30 AG038072, 5T32AG023475–20 from the NIA, and R01CA214625, R01CA229216, R01CA222358, and P30-013330 from the NCI.

CONFLICT OF INTEREST STATEMENT

All authors state that there is no conflict of interest.

DATA AVAILABILITY STATEMENT

scRNAseq data sets have been deposited in the Gene Expression Omnibus (GEO) database under the accession code: GSE210669.

ORCID

Jiahn Choi https://orcid.org/0000-0001-7344-767X

REFERENCES

Alonso, S., & Yilmaz, O. H. (2018). Nutritional regulation of intestinal stem cells. *Annual Review of Nutrition*, *38*, 273–301. https://doi.org/10.1146/annurev-nutr-082117-051644

An, J. Y., Kerns, K. A., Ouellette, A., Robinson, L., Morris, H. D., Kaczorowski, C., Park, S. I., Mekvanich, T., Kang, A., McLean, J., Cox, T. C., & Kaeberlein, M. (2020). Rapamycin rejuvenates oral health in aging mice. *eLife*, *9*, e54318. https://doi.org/10.7554/eLife.54318

Aslam, M. N., Paruchuri, T., Bhagavathula, N., & Varani, J. (2010). A mineral-rich red algae extract inhibits polyp formation and inflammation in the gastrointestinal tract of mice on a high-fat diet. *Integrative Cancer Therapies*, *9*(1), 93–99. https://doi.org/10.1177/1534735409360360

Augenlicht, L. H., & Heerdt, B. G. (2001). Mitochondria: Integrators in tumorigenesis? *Nature Genetics*, *28*(2), 104–105. https://doi.org/10.1038/88800

Barker, N., van Es, J. H., Kuipers, J., Kujala, P., van den Born, M., Cozijnsen, M., Haegebarth, A., Korving, J., Begthel, H., Peters, P. J., & Clevers, H. (2007). Identification of stem cells in small intestine and colon by marker gene Lgr5. *Nature*, *449*(7165), 1003–1007. https://doi.org/10.1038/nature06196

Baron, B., & Pisani, G. (2021). Mechanisms causing aging, current knowledge and the way forward. *Journal of Advances in Medicine and Medical Research*, *33*, 233–250. https://doi.org/10.9734/jammr/2021/v33i2131152

Beumer, J., & Clevers, H. (2020). Cell fate specification and differentiation in the adult mammalian intestine. *Nature Reviews. Molecular Cell Biology*, *22*, 39–53. https://doi.org/10.1038/s41580-020-0278-0

Blagosklonny, M. V. (2019). Rapamycin for the Aging Skin. *Aging (Albany NY)*, *11*(24), 12822–12826. https://doi.org/10.18632/aging.102664

Chandel, N. S., Jasper, H., Ho, T. T., & Passegue, E. (2016). Metabolic regulation of stem cell function in tissue homeostasis and organismal ageing. *Nature Cell Biology*, *18*(8), 823–832. https://doi.org/10.1038/ncb3385

Choi, J., Rakhilin, N., Gadamsetty, P., Joe, D. J., Tabrizian, T., Lipkin, S. M., Huffman, D. M., Shen, X., & Nishimura, N. (2018). Intestinal crypts recover rapidly from focal damage with coordinated motion of stem cells that is impaired by aging. *Scientific Reports*, *8*(1), 10989. https://doi.org/10.1038/s41598-018-29230-y

Choi, J., Zhang, X., Li, W., Houston, M., Peregrina, K., Dubin, R., Ye, K., & Augenlicht, L. H. (2022). Dietary induced dynamic plasticity of intestinal stem cells and the mucosa in elevating risk for tumor development. *Preprint at bioRxiv*. https://doi.org/10.1101/2022.03.17.484800

Cui, H., Tang, D., Garside, G. B., Zeng, T., Wang, Y., Tao, Z., Zhang, L., & Tao, S. (2019). Wnt signaling mediates the aging-induced differentiation impairment of intestinal stem cells. *Stem Cell Reviews and Reports*, *15*(3), 448–455. https://doi.org/10.1007/s12015-019-09880-9

Di Giosia, P., Stamerra, C. A., Giorgini, P., Jamialahamdi, T., Butler, A. E., & Sahebkar, A. (2022). The role of nutrition in inflammaging. *Ageing Research Reviews*, *77*, 101596. https://doi.org/10.1016/j.arr.2022.101596

Harrison, D. E., Strong, R., Sharp, Z. D., Nelson, J. F., Astle, C. M., Flurkey, K., Nadon, N. L., Wilkinson, J. E., Frenkel, K., Carter, C. S., Pahor, M., Javors, M. A., Fernandez, E., & Miller, R. A. (2009). Rapamycin fed late in life extends lifespan in genetically heterogeneous mice. *Nature*, *460*(7253), 392–395. https://doi.org/10.1038/nature08221

He, D., Wu, H., Xiang, J., Ruan, X., Peng, P., Ruan, Y., Chen, Y. G., Wang, Y., Yu, Q., Zhang, H., Habib, S. L., de Pinho, R. A., Liu, H., & Li, B. (2020). Gut stem cell aging is driven by mTORC1 via a p38 MAPK-p53 pathway. *Nature Communications*, *11*(1), 37. https://doi.org/10.1038/s41467-019-13911-x

Li, W., Zimmerman, S. E., Peregrina, K., Houston, M., Mayoral, J., Zhang, J., Maqbool, S., Zhang, Z., Cai, Y., Ye, K., & Augenlicht, L. H. (2019). The nutritional environment determines which and how intestinal stem cells contribute to homeostasis and tumorigenesis. *Carcinogenesis*, *40*(8), 937–946. https://doi.org/10.1093/carcin/bgz106

Ludikhuize, M. C., Meerlo, M., Gallego, M. P., Xanthakis, D., Burgaya Julià, M., Nguyen, N. T. B., Brombacher, E. C., Liv, N., Maurice, M. M., Paik, J. H., Burgering, B. M. T., & Rodriguez Colman, M. J. (2020). Mitochondria define intestinal stem cell differentiation downstream of a FOXO/notch Axis. *Cell Metabolism*, *32*(5), 889–900 e887. https://doi.org/10.1016/j.cmet.2020.10.005

Mariadason, J. M., Nicholas, C., L'Italien, K. E., Zhuang, M., Smartt, H. J. M., Heerdt, B. G., Yang, W., Corner, G. A., Wilson, A. J., Klampfer, L., Arango, D., & Augenlicht, L. H. (2005). Gene expression profiling of intestinal epithelial cell maturation along the crypt-villus axis. *Gastroenterology*, *128*(4), 1081–1088. https://doi.org/10.1053/j.gastro.2005.01.054

Martin-Montalvo, A., Mercken, E. M., Mitchell, S. J., Palacios, H. H., Mote, P. L., Scheibye-Knudsen, M., Gomes, A. P., Ward, T. M., Minor, R. K., Blouin, M. J., Schwab, M., Pollak, M., Zhang, Y., Yu, Y., Becker, K. G., Bohr, V. A., Ingram, D. K., Sinclair, D. A., Wolf, N. S., … de Cabo, R. (2013). Metformin improves healthspan and lifespan in mice. *Nature Communications*, *4*, 2192. https://doi.org/10.1038/ncomms3192

Massey, F. J., Jr. (1951). The Kolmogorov-Smirnov test for goodness of fit. *Journal of the American Statistical Association*, *46*, 68–78. https://doi.org/10.1080/01621459.1951.10500769

Mihaylova, M. M., Cheng, C. W., Cao, A. Q., Tripathi, S., Mana, M. D., Bauer-Rowe, K. E., Abu-Remaileh, M., Clavain, L., Erdemir, A., Lewis, C. A., Freinkman, E., Dickey, A. S., la Spada, A. R., Huang, Y., Bell, G. W., Deshpande, V., Carmeliet, P., Katajisto, P., Sabatini, D. M., & Yilmaz, Ö. H. (2018). Fasting activates fatty acid oxidation to enhance intestinal stem cell function during homeostasis and aging. *Cell Stem Cell*, *22*(5), 769–778 e764. https://doi.org/10.1016/j.stem.2018.04.001

Moor, A. E., Harnik, Y., Ben-Moshe, S., Massasa, E. E., Rozenberg, M., Eilam, R., Bahar Halpern, K., & Itzkovitz, S. (2018). Spatial reconstruction of single enterocytes uncovers broad zonation along the intestinal villus Axis. *Cell*, *175*(4), 1156–1167 e1115. https://doi.org/10.1016/j.cell.2018.08.063

Moskalev, A. (2020). Is anti-ageing drug discovery becoming a reality? *Expert Opinion on Drug Discovery*, *15*(2), 135–138. https://doi.org/10.1080/17460441.2020.1702965

Moskalev, A., Guvatova, Z., Lopes, I. A., Beckett, C. W., Kennedy, B. K., De Magalhaes, J. P., & Makarov, A. A. (2022). Targeting aging

mechanisms: Pharmacological perspectives. *Trends in Endocrinology and Metabolism*, *33*, 266–280. https://doi.org/10.1016/j.tem.2022.01.007

Muñoz, J., Stange, D. E., Schepers, A. G., van de Wetering, M., Koo, B. K., Itzkovitz, S., Volckmann, R., Kung, K. S., Koster, J., Radulescu, S., Myant, K., Versteeg, R., Sansom, O. J., van Es, J., Barker, N., van Oudenaarden, A., Mohammed, S., Heck, A. J., & Clevers, H. (2012). The Lgr5 intestinal stem cell signature: Robust expression of proposed quiescent '+4′ cell markers. *The EMBO Journal*, *31*(14), 3079–3091. https://doi.org/10.1038/emboj.2012.166

Nalapareddy, K., Nattamai, K. J., Kumar, R. S., Karns, R., Wikenheiser-Brokamp, K. A., Sampson, L. L., Mahe, M. M., Sundaram, N., Yacyshyn, M. B., Yacyshyn, B., Helmrath, M. A., Zheng, Y., & Geiger, H. (2017). Canonical Wnt signaling ameliorates aging of intestinal stem cells. *Cell Reports*, *18*(11), 2608–2621. https://doi.org/10.1016/j.celrep.2017.02.056

Nalapareddy, K., Zheng, Y., & Geiger, H. (2022). Aging of intestinal stem cells. *Stem Cell Reports*, *17*, 734–740. https://doi.org/10.1016/j.stemcr.2022.02.003

Newmark, H. L., Yang, K., Kurihara, N., Fan, K., Augenlicht, L. H., & Lipkin, M. (2009). Western-style diet-induced colonic tumors and their modulation by calcium and vitamin D in C57Bl/6 mice: A preclinical model for human sporadic colon cancer. *Carcinogenesis*, *30*(1), 88–92. https://doi.org/10.1093/carcin/bgn229

Newmark, H. L., Yang, K., Lipkin, M., Kopelovich, L., Liu, Y., Fan, K., & Shinozaki, H. (2001). A Western-style diet induces benign and malignant neoplasms in the colon of normal C57Bl/6 mice. *Carcinogenesis*, *22*(11), 1871–1875. https://doi.org/10.1093/carcin/22.11.1871

Novelle, M. G., Ali, A., Dieguez, C., Bernier, M., & de Cabo, R. (2016). Metformin: A hopeful promise in aging research. *Cold Spring Harbor Perspectives in Medicine*, *6*(3), a025932. https://doi.org/10.1101/cshperspect.a025932

Partridge, L., Fuentealba, M., & Kennedy, B. K. (2020). The quest to slow ageing through drug discovery. *Nature Reviews. Drug Discovery*, *19*(8), 513–532. https://doi.org/10.1038/s41573-020-0067-7

Pentinmikko, N., Iqbal, S., Mana, M., Andersson, S., Cognetta, A. B., 3rd, Suciu, R. M., Roper, J., Luopajärvi, K., Markelin, E., Gopalakrishnan, S., Smolander, O. P., Naranjo, S., Saarinen, T., Juuti, A., Pietiläinen, K., Auvinen, P., Ristimäki, A., Gupta, N., Tammela, T., … Katajisto, P. (2019). Notum produced by Paneth cells attenuates regeneration of aged intestinal epithelium. *Nature*, *571*(7765), 398–402. https://doi.org/10.1038/s41586-019-1383-0

Rodríguez-Colman, M. J., Schewe, M., Meerlo, M., Stigter, E., Gerrits, J., Pras-Raves, M., Sacchetti, A., Hornsveld, M., Oost, K. C., Snippert, H. J., Verhoeven-Duif, N., Fodde, R., & Burgering, B. M. (2017). Interplay between metabolic identities in the intestinal crypt supports stem cell function. *Nature*, *543*(7645), 424–427. https://doi.org/10.1038/nature21673

Smillie, C. S., Biton, M., Ordovas-Montanes, J., Sullivan, K. M., Burgin, G., Graham, D. B., Herbst, R. H., Rogel, N., Slyper, M., Waldman, J., Sud, M., Andrews, E., Velonias, G., Haber, A. L., Jagadeesh, K., Vickovic, S., Yao, J., Stevens, C., Dionne, D., … Regev, A. (2019). Intra- and inter-cellular rewiring of the human Colon during ulcerative colitis. *Cell*, *178*(3), 714–730 e722. https://doi.org/10.1016/j.cell.2019.06.029

Stuart, T., Butler, A., Hoffman, P., Hafemeister, C., Papalexi, E., Mauck, W. M., 3rd, Hao, Y., Stoeckius, M., Smibert, P., & Satija, R. (2019). Comprehensive integration of single-cell data. *Cell*, *177*(7), 1888–1902 e1821. https://doi.org/10.1016/j.cell.2019.05.031

Tirosh, I., Izar, B., Prakadan, S. M., Wadsworth, M. H., 2nd, Treacy, D., Trombetta, J. J., Rotem, A., Rodman, C., Lian, C., Murphy, G., Fallahi-Sichani, M., Dutton-Regester, K., Lin, J. R., Cohen, O., Shah, P., Lu, D., Genshaft, A. S., Hughes, T. K., Ziegler, C. G., … Garraway, L. A. (2016). Dissecting the multicellular ecosystem of metastatic melanoma by single-cell RNA-seq. *Science*, *352*(6282), 189–196. https://doi.org/10.1126/science.aad0501

Trapnell, C., Cacchiarelli, D., Grimsby, J., Pokharel, P., Li, S., Morse, M., Lennon, N. J., Livak, K. J., Mikkelsen, T. S., & Rinn, J. L. (2014). The dynamics and regulators of cell fate decisions are revealed by pseudotemporal ordering of single cells. *Nature Biotechnology*, *32*(4), 381–386. https://doi.org/10.1038/nbt.2859

Wang, D., Odle, J., & Liu, Y. (2021). Metabolic regulation of intestinal stem cell homeostasis. *Trends in Cell Biology*, *31*, 325–327. https://doi.org/10.1016/j.tcb.2021.02.001

Yang, K., Kurihara, N., Fan, K., Newmark, H., Rigas, B., Bancroft, L., Corner, G., Livote, E., Lesser, M., Edelmann, W., Velcich, A., Lipkin, M., & Augenlicht, L. (2008). Dietary induction of colonic tumors in a mouse model of sporadic colon cancer. *Cancer Research*, *68*(19), 7803–7810. https://doi.org/10.1158/0008-5472.CAN-08-1209

Zhang, W., Li, J., Duan, Y., Li, Y., Sun, Y., Sun, H., Yu, X., Gao, X., Zhang, C., Zhang, H., Shi, Y., & He, X. (2022). Metabolic regulation: A potential strategy for rescuing stem cell senescence. *Stem Cell Reviews and Reports*, *18*, 1728–1742. https://doi.org/10.1007/s12015-022-10348-6

SUPPORTING INFORMATION

Additional supporting information can be found online in the Supporting Information section at the end of this article.

How to cite this article: Choi, J., Houston, M., Wang, R., Ye, K., Li, W., Zhang, X., Huffman, D M., & Augenlicht, L H. (2023). Intestinal stem cell aging at single-cell resolution: Transcriptional perturbations alter cell developmental trajectory reversed by gerotherapeutics. *Aging Cell*, *22*, e13802. https://doi.org/10.1111/acel.13802